Neuron, Volume *94*

Supplemental Information

Dorsal Raphe Dopamine Neurons Modulate Arousal and Promote Wakefulness by Salient Stimuli

Jounhong Ryan Cho, Jennifer B. Treweek, J. Elliott Robinson, Cheng Xiao, Lindsay R. Bremner, Alon Greenbaum, and Viviana Gradinaru

Supplemental Figure Legend

Figure S1: related to all main figures.
(A) Schematic of a fiber photometry setup. See Supplementary Experimental Procedures for details.
(B) Representative trace from a $DRN^{DA\text{-}GCaMP6f}$ mouse that shows dynamic Ca^{2+}-dependent fluorescence across time.
(C) Representative trace from a $DRN^{DA\text{-}eGFP}$ mouse. Notice minimal fluctuations in fluorescence.
(D) Confocal image of serotonin (5-HT, green) and dopamine (TH, red) neurons in the DRN. Notice that there is no overlap between the two populations and that the number of TH+ neurons is far less than that of 5-HT+ neurons. Scale bar is 100 μm.
(E) Viral expression of diverse transgenes did not affect normal sleep-wake architecture both in light (left) and dark (right) phases (n = 4 per group; one-way ANOVA, all $p > 0.2$).
(F) Time spent in each state per hour in 24-hour recordings: Wake (left), NREM (middle), and REM sleep (right).
(G) Representative confocal image of GCaMP6f+ neurons in the DRN and the location of fiber-tip (in this case, for fiber photometry). Scale bar is 100 μm.
(H) Histologically verified fiber-tip locations of $DRN^{DA\text{-}GCaMP6f}$ (dark blue), $DRN^{DA\text{-}GCaMP6s}$ (green), $DRN^{DA\text{-}ChR2}$ (sky blue), $DRN^{DA\text{-}eGFP}$ (orange), and $DRN^{DA\text{-}Arch}$ (yellow) mice.
Data are represented as mean ± s.e.m.

Figure S2: related to Figure 1.
(A) Left, social interaction between a male $DRN^{DA\text{-}GCaMP6f}$ resident mouse and a male juvenile intruder were associated with increased DRN^{DA} activity. Right, quantification of the area under the curve per second (AUC) showed that DRN^{DA} activity during first interaction (0 – 5 s) was significantly increased compared with baseline (-5 – 0 s) (n = 7 $DRN^{DA\text{-}GCaMP6f}$ mice, paired t-test, $t_6 = 4.679$, $^{**}p < 0.01$).
(B) Left, attack/fight bouts (first bout only) between a male $DRN^{DA\text{-}GCaMP6f}$ resident and an adult intruder were associated with increased DRN^{DA} activity. Right, DRN^{DA} activity during attack (0 – 5 s) was significantly increased relative to baseline (-5 – 0 s) (n = 4 $DRN^{DA\text{-}GCaMP6f}$ mice, paired t-test, $t_3 = 4.993$, $^{*}p < 0.05$).
(C) Left, brief air puffs (<1 s) were intermittently delivered to the tail of a $DRN^{DA\text{-}GCAMP6f}$ mouse, which caused time-locked DRN^{DA} fluorescence increase. Right, DRN^{DA} activity after air puff delivery (0 – 5 s) was significantly increased relative to baseline (-5 – 0 s) (n = 7 $DRN^{DA\text{-}GCaMP6f}$ mice; paired t-test, $t_6 = 7.518$, $^{***}p < 0.001$).
(D) Left, fiber photometry recording of $DRN^{DA\text{-}GCaMP6f}$ mice undergoing a 5-minute tail suspension test. DRN^{DA} neurons showed time-locked activation at the onset of mobility or struggling. Right, AUC values during mobility (0 – 5 s) were significantly increased compared with baseline (-5 – 0 s) (n = 7 $DRN^{DA\text{-}GCaMP6f}$ mice, paired t-test, $t_6 = 3.044$, $^{*}p < 0.05$).
(E) Left, investigation of predator odor TMT was associated with increase in DRN^{DA} activity. Right, quantification of the AUC showed that there was significant difference in DRN^{DA} activity between interaction (0 – 5 s) and baseline (-5 – 0 s) (n = 7 $DRN^{DA\text{-}GCaMP6f}$ mice, paired t-test, $t_6 = 2.653$, $^{*}p < 0.05$).
(F) Left, there was a prolonged increase in DRN^{DA} neuronal activity while a $DRN^{DA\text{-}GCaMP6f}$ mouse was restrained or immobilized. Right, sustained activation of DRN^{DA} neurons was observed throughout the restraint period (0 – 60 s), compared baseline (-60 – 0 s) (n = 6 $DRN^{DA\text{-}GCaMP6f}$ mice, paired t-test, $t_5 = 5.444$, $^{**}p < 0.01$).
(G) Left, averaged DRN^{DA} activity was increased during second and third interaction bouts (red trace), when a resident male $DRN^{DA\text{-}GCaMP6f}$ mouse was investigating a female intruder. Photometry data from first interaction (black trace, Fig 1D) was also illustrated for comparison. Right, AUC values during second and third interaction bouts (0 – 5 s) were significantly

increased relative to baseline (-5 – 0 s) (n = 7 $DRN^{DA\text{-}GCaMP6f}$ mice, paired t-test, $t_6 = 4.437$, **p < 0.01).
(H) Left, averaged DRN^{DA} activity was increased during the second and third episodes of aggression (red trace) by a resident male $DRN^{DA\text{-}GCaMP6f}$ mouse against a male intruder. Photometry data from the first attack episode (black trace, Fig. S2B) was also illustrated for comparison. Right, quantification of AUC revealed that DRN^{DA} activity during the second and third episodes of attack (0 – 5 s) was significantly increased relative to baseline (-5 – 0 s) (n = 4 $DRN^{DA\text{-}GCaMP6f}$ mice, paired t-test, $t_3 = 3.235$, *p < 0.05).
(I) Left, averaged DRN^{DA} activity during the second and third investigation bouts (red trace) in novel object interaction assays was not different from preceding baseline. Photometry data from first interaction bout (black trace, Fig. 1J) was also illustrated for comparison. Right, quantification of the area under the curve per second (AUC) showed that DRN^{DA} activity during the second and third interactions with a novel object (0 – 5 s) was not significantly increased compared with baseline (-5 – 0 s) (n = 7 $DRN^{DA\text{-}GCaMP6f}$ mice, paired t-test, $t_6 = 2.406$, p > 0.05).
(J) Left, a robust increase in DRN^{DA} activity during the first interaction bout with a female mouse was observed in both single-housed (black, Fig. 1D) and group-housed (purple) mice. Right, quantification of AUC values during interaction (0 – 5 s) from single-housed and group-housed mice showed that there was no significant difference in DRN^{DA} activity based on housing conditions (n = 7 single-housed, n = 4 group-housed $DRN^{DA\text{-}GCaMP6f}$ mice; unpaired t-test, p > 0.1).
(K) Left, time-locked DRN^{DA} activation was present when single-housed (black, Fig. 1H) and group-housed (purple) mice received unexpected electric footshocks. Right, AUC values during footshock delivery did not differ between single- and group-housed mice (n = 7 single-housed, n = 4 group-housed $DRN^{DA\text{-}GCaMP6f}$ mice; unpaired t-test, p > 0.7).
(L) Left, small DRN^{DA} activation was observed in the first interaction bout with a novel object in both single-housed (black, Fig. 1J) and group-housed (purple) mice. Right, AUC values during novel object interaction were not distinct between single- and group-housed mice (n = 7 single-housed, n = 4 group-housed $DRN^{DA\text{-}GCaMP6f}$ mice; unpaired t-test, p > 0.5).
(M) Representative fiber photometry recording (black: fluorescence trace) and real-time locomotion tracking (red: velocity) for a $DRN^{DA\text{-}GCaMP6f}$ mouse during the open field test. Notice the lack of temporal correlation between two signals.
(N) Averaged velocities aligned by detected Ca^{2+} peak event onset showed that increased DRN^{DA} activity is not associated with any change in velocity.
(O) Averaged DRN^{DA} activity aligned by detected locomotion onset revealed that locomotion onset (indexed by increase of velocity) was not associated with a change in DRN^{DA} fluorescence.
Data are represented as mean ± s.e.m.

Figure S3: related to Figure 2 and 3.
(A) Representative example of a REM-to-wake transition from a $DRN^{DA\text{-}GCaMP6s}$ mouse with EEG spectrogram, EEG, EMG, and fiber photometry traces. Note that DRN^{DA} fluorescence was increased at the wake onset, when EEG shifted from theta oscillations (5-10 Hz) to desynchronized rhythms and EMG amplitude abruptly increased.
(B) Same as (A), but from a $DRN^{DA\text{-}eGFP}$ mouse. No change in fiber photometry signal is observed.
(C) Power spectral density plots of $DRN^{DA\text{-}GCaMP6s}$ mice at each state: wake (blue), NREM (red), and REM (green). Notice that they show normal spectral EEG characteristics at each state: wake is characterized by smaller low-frequency activity and elevated high-frequency activity, NREM is characterized by high delta or slow wave (0.5-4 Hz) activity with suppressed high-frequency rhythms, and REM is associated with high theta (5-10 Hz) peak with elevated high-frequency activity.

(D) Even with constant LED light exposure for exciting GCaMP6s, $DRN^{DA\text{-}GCaMP6s}$ mice showed normal sleep-wake architecture during light phase when synchronized photometry and EEG/EMG recordings were performed. Left, time spent at each state (For comparison, please see Fig. S1E). Right, mean duration of each state.
(E) After aligning the linearly scaled control 405 nm signal (red) with the 490 nm signal (blue), no noticeable decay was detected in the quality or signal-to-noise ratio of an extended photometry trace (black, 12-hour recording).
(F) A representative photometry recording from a $DRN^{DA\text{-}GCaMP6s}$ mouse, with examples of automatically detected Ca^{2+} peak events (red). Detection onsets are denoted with black asterisks.
(G) The frequency of detected peak events per 5-second window did not vary across sleep-wake states (n = 6 $DRN^{DA\text{-}GCaMP6s}$ mice; one-way ANOVA, $F_{2,15} = 0.07802$, $p > 0.9$).
(H) Duration of the detected peak events did not vary significantly across sleep-wake states (n = 6 $DRN^{DA\text{-}GCaMP6s}$ mice; one-way ANOVA, $F_{2,15} = 0.2999$, $p > 0.7$).
(I) Amplitude (z-scored) of the detected peak events was significantly increased in wake compared to NREM sleep (n = 6 $DRN^{DA\text{-}GCaMP6s}$ mice; one-way ANOVA, $F_{2,15} = 7.144$, $p < 0.01$; Post-hoc Bonferroni Analysis, $^{**}p < 0.01$)
(J) Summed area under curve values within a 5-sec window was significantly increased at wake state over NREM and REM sleep (n = 6 $DRN^{DA\text{-}GCaMP6s}$ mice; one-way ANOVA, $F_{2,15} = 15.59$, $p < 0.001$; Post-hoc Bonferroni Analysis, $^{**}p < 0.01$, $^{***}p < 0.001$).
(K) To additionally confirm that wake DRN^{DA} dynamics (activity peak soon after onset and gradual decrease, see Figure 2H) did not originate from photo-bleaching, we only isolated the wake episodes whose durations were similar to NREM and REM sleep episode durations (between 25^{th} and 75^{th} percentile of the sleep duration distribution, which were 80 and 260 seconds respectively) and plotted the normalized fluorescence over normalized time similar to Figure 2H. We observe the similar trend, suggesting that the observed wake dynamics is unique to DRN^{DA} neurons and that the contribution from photo-bleaching is minimal.
(L) Left, when mice made transitions from REM sleep to NREM sleep through a short period of arousal (wake shorter than 15 seconds), the DRN^{DA} activity decreased. Right, Quantification of the area under the curve per second showed that DRN^{DA} activity was significantly lower after transitions than before transitions (n = 6 $DRN^{DA\text{-}GCaMP6s}$ mice, paired t-test, $t_5 = 2.823$, $^{*}p < 0.05$). Data are represented as mean ± s.e.m.

Figure S4, related to Figure 4.
(A) *Ex vivo* patch clamp recording demonstrated that DRN^{DA} neurons could faithfully follow our parameters of phasic stimulation (30 Hz, 10 pulses, 10 ms pulse width).
(B) Representative EEG (black) and EMG (gray) recordings when phasic DRN^{DA} stimulation caused immediate (<5 second) NREM-to-wake transitions in a $DRN^{DA\text{-}ChR2}$ mouse. Notice the termination of slow delta waves and abrupt increase of muscle activity after a phasic pulse. The same phasic stimulation paradigm did not cause any state changes in a $DRN^{DA\text{-}eGFP}$ mouse.
(C) Same as (B), but when phasic stimulation occurred during REM sleep.
(D) Two-minute tonic stimulations (continuous 2 Hz pulses for 2 minutes, 10 ms pulse width) were delivered every 20-25 minutes to $DRN^{DA\text{-}ChR2}$ and $DRN^{DA\text{-}eGFP}$ mice.
(E) Tonic stimulation caused a small increase in the wake probability and a small decrease in the NREM and REM probability in $DRN^{DA\text{-}ChR2}$ mice.
(F) No changes were observed upon tonic stimulation in $DRN^{DA\text{-}eGFP}$ mice.
(G) REM state probability was significantly decreased in $DRN^{DA\text{-}ChR2}$ mice compared to $DRN^{DA\text{-}eGFP}$ mice (n = 8 $DRN^{DA\text{-}ChR2}$ mice, n = 7 $DRN^{DA\text{-}eGFP}$ mice; unpaired t-test, $^{*}p < 0.05$). Although $DRN^{DA\text{-}ChR2}$ mice appeared to spend more time in the wake state, this trend did not reach statistical significance (unpaired t-test, $p = 0.057$). There were no significant differences in NREM state probability change between two groups (unpaired t-test, $p > 0.3$).

(H) Power spectral density of $DRN^{DA\text{-}ChR2}$ mice (see Figure 4H), but divided into low (0.5-30 Hz) and high (40-100 Hz) frequency ranges for better visualization.
(I) Same as (H), but for power spectral density of $DRN^{DA\text{-}eGFP}$ mice (see Figure 4I).
(J) Wake-promoting effect of DRN^{DA} activation was abolished with systemic administration of D1 and D2 receptor antagonists. D1/D2 antagonists injection resulted in a significant decrease of the time spent awake (n = 4 $DRN^{DA\text{-}ChR2}$ mice; paired t-test, $t_3 = 7.161$, $^{**}p<0.01$) and a significant increase in the time spent in NREM (paired t-test, $t_3 = 5.796$, $^{*}p<0.05$) and REM sleep (paired t-test, $t_3 = 6.673$, $^{**}p<0.01$), compared to saline injection.
(K) $DRN^{DA\text{-}eGFP}$ mice showed no significant change in the time spent in any state (n = 4 $DRN^{DA\text{-}eGFP}$ mice, paired t-test, all $p>0.4$) after systemic administration of saline or D1/D2 antagonists.
(L) $DRN^{DA\text{-}ChR2}$ and $DRN^{DA\text{-}eGFP}$ mice underwent the open field test at the dark and light phases to examine the causal effect of DRN^{DA} activation with locomotion. There was no difference in distance traveled in the open field between the two mouse groups across light OFF and ON epochs in both phases(n = 6 per group; two-way ANOVA revealed no light x epoch interaction in both phases, $F_{2,20}$ (dark) = 0.089, $p > 0.9$, $F_{2,20}$ (light) = 2.088, $p > 0.1$).
(M) Real-time place preference/aversion assay with $DRN^{DA\text{-}ChR2}$ and $DRN^{DA\text{-}eGFP}$ mice demonstrated that $DRN^{DA\text{-}ChR2}$ mice spent less time in the chamber paired with phasic light stimulation, but this trend for place aversion was not statistically different from $DRN^{DA\text{-}eGFP}$ mice group place preference/aversion (n = 6 per group; unpaired t-test, $p > 0.1$).
(N) Virus injection into the DRN results in the transgene expression in the caudal linear nucleus (CLi) but not in the retrotrubral field (RRF). Scale bar is 1 mm.
(O) Virus injection into the DRN does not result in cell-body expression, but show fibers (originating from DRN) in the VTA or SNc. Scale bar is 1 mm.
(P) ChR2-eYFP fibers were found in the basolateral amygdala (BLA) and the central nucleus of the amygdala (CeA).
(Q) Bed nucleus of the stria terminalis (BNST).
(R) Caudal part of nucleus accumbens (NAc).
(S) Medial prefrontal cortex (mPFC). All scale bars from (P) to (S) are 500 μm.
Data are represented as mean ± s.e.m.

Figure S5, related to Figure 5.
(A) Images of DIC (upper) and fluorescence (lower) from a patched DRN^{DA} neuron expressing hM4Di-mCherry.
(B) Representative example recording of membrane potentials from an hM4Di+ DRN^{DA} neuron. Bath application of CNO (1 uM) resulted in hyperpolarization and a reduction of neuronal firing, which was recovered after washout. Holding potential was at -45 mV.
(C) Same as (B), but for an eGFP+ DRN^{DA} neuron. Notice that there was no detectable change in membrane potential or firing rate. Holding potential was at -45 mV.
(D) Application of CNO reduced the membrane potential of hM4Di+ neurons, but not in eGFP+ neurons. (n = 4 cells each; unpaired t-test, $^{*}p < 0.05$). Baseline was defined as 1-minute epoch before CNO application, and CNO induced change was quantified from 2 to 4 minutes after CNO bath application.
(E) Firing rate was significantly reduced with CNO application in hM4Di+ neurons, relative to eGFP+ neurons (n = 4 cells each; unpaired t-test, $^{**}p < 0.01$).
(F-I) Stereotaxic injection of AAV2-hSyn-DIO-hM4Di-mCherry (red) vectors into the DRN of TH-Cre mice did not result in anterograde or retrograde transport to other TH+ neurons (green) in **(F)** locus coeruleus (LC), **(G)** retrorubral field (RRF), **(H)** ventral tegmental area (VTA), and **(I)** substantia nigra pars compacta (SNc) after one month. Axonal fibers (presumably coming from the DRN^{DA} neurons) were shown, but no cell body expression was present in these areas. Scale bars are 100 um.

(J) Power spectral density during wakefulness from $DRN^{DA\text{-}hM4Di}$ mice after saline (blue) and CNO (red) injection. Notice that EEG spectra after CNO delivery were not distinct from saline controls.
(K) Same as (J), but for NREM sleep.
(L) Same as (J), but for REM sleep.
Data are represented as mean ± s.e.m.

Figure S6, related to Figure 6.
(A) Fiber photometry and EEG/EMG recordings were performed in $DRN^{DA\text{-}GCaMP6s}$ mice. Arousing auditory tones (65 dB, 2-5 kHz, 2 Hz pulse frequency, 250 ms pulse, for 10 seconds) were randomly triggered during the light phase.
(B) The presentation of auditory cues was associated with a time-locked increase in DRN^{DA} activity, especially in sleep-to-wake transitions.
(C) DRN^{DA} activity change, as indexed by the difference in the area under the curve between before (-30-0 s) and after (0-30 s) tone presentation, was larger when the auditory tone induced sleep-to-wake transitions (within 10 seconds) than when it was turned on during the wake state or when it failed to cause sleep-to-wake transitions (n = 7 $DRN^{DA\text{-}GCaMP6s}$ mice; one-way ANOVA, $F_{2,18} = 10.79$, $p < 0.001$, Bonferroni post-hoc analysis, *$p < 0.05$, ***$p < 0.001$).
(D) Increased DRN^{DA} population activity was observed when arousing tones woke up $DRN^{DA\text{-}GCaMP6s}$ mice from NREM (red) or REM (green) sleep states.
(E) The time-locked increase in DRN^{DA} activity upon auditory tone presentation did not vary according to the type of sleep-to-wake transitions (NREM-to-wake versus REM-to wake; n = 7 $DRN^{DA\text{-}GCaMP6s}$ mice, paired t-test, $t_6 = 1.4094$, $p > 0.2$).
(F) EEG/EMG monitoring was performed with $DRN^{DA\text{-}Arch}$ or $DRN^{DA\text{-}hM4Di}$ mice while auditory tones (70 dB) were turned on during the light phase. Green laser (532 nm) was applied for 20 seconds surrounding the tonal stimuli for time-locked DRN^{DA} inhibition.
(G) Confocal images of Arch+ (green) neurons co-localized with TH (red) expression. Scale bar is 100 μm.
(H) There was a noticeable decrease in delta (0.5-4 Hz) amplitude in NREM-to-wake trials (blue), when auditory cues successfully caused wake transitions from NREM sleep, whereas there was minimal change of delta (0.5-4 Hz) amplitude in NREM-to-NREM trials (red), when auditory cues failed to cause wake transitions from NREM. Data are pooled together from both $DRN^{DA\text{-}Arch}$ and $DRN^{DA\text{-}eGFP}$ mice.
(I) There was no difference in delta (0.5-4 Hz) amplitude before and after tones in NREM-to-NREM trials (n = 67 trials; paired t-test, $t_{66} = 1.310$, $p > 0.1$). However, there was significant decrease in delta (0.5-4 Hz) amplitude across tones in NREM-to-wake trials (n = 123 trials; paired t-test, $t_{122} = 10.58$, ***$p < 0.0001$).
(J) There was a noticeable decrease in theta (5-10 Hz) amplitude in REM-to-wake trials (blue), when auditory cues successfully caused wake transitions from REM sleep, while there was minimal change of theta (5-10 Hz) amplitude in REM-to-REM trials (red), when auditory cues failed to cause wake transitions from REM trials. Data are pooled together from both $DRN^{DA\text{-}Arch}$ and $DRN^{DA\text{-}eGFP}$ mice.
(K) There was no difference in theta (5-10 Hz) amplitude before and after tones in REM-to-REM trials (n = 5 trials; paired t-test, $t_4 = 0.2832$, $p > 0.7$). However, there was significant decrease in theta amplitude across tones in REM-to-wake trials (n = 30 trials; paired t-test, $t_{29} = 5.786$, ***$p < 0.0001$).
(L) The probability of NREM-to-wake transitions upon auditory tones was significantly lower in $DRN^{DA\text{-}Arch}$ mice compared to $DRN^{DA\text{-}eGFP}$ mice (n = 6 $DRN^{DA\text{-}Arch}$ mice, n = 4 $DRN^{DA\text{-}eGFP}$ mice; unpaired t-test, $p < 0.001$).
(M) Left, delta (0.5-4 Hz) amplitude decrease was less prominent in $DRN^{DA\text{-}Arch}$ mice compared to control mice. Right, delta (0.5-4 Hz) amplitude during the tone was significantly higher in

$DRN^{DA\text{-}Arch}$ mice than $DRN^{DA\text{-}eGFP}$ controls (n = 6 $DRN^{DA\text{-}Arch}$ mice, n = 4 $DRN^{DA\text{-}eGFP}$ mice; unpaired t-test, *p < 0.05).
(N) The probability of REM-to-wake transitions upon auditory tones presentation was not different between $DRN^{DA\text{-}Arch}$ and $DRN^{DA\text{-}eGFP}$ mice (n = 6 $DRN^{DA\text{-}Arch}$ mice, n = 4 $DRN^{DA\text{-}eGFP}$ mice; unpaired t-test, p > 0.1).
(O) Left, the decrease in theta (5-10 Hz) amplitude was similar between $DRN^{DA\text{-}Arch}$ and $DRN^{DA\text{-}eGFP}$ mice. Right, there was no statistically detectable difference in the theta (5-10 Hz) amplitude between groups during the tone presentation (n = 6 $DRN^{DA\text{-}Arch}$ mice, n = 4 $DRN^{DA\text{-}eGFP}$ mice; unpaired t-test, p > 0.6).

Figure S1

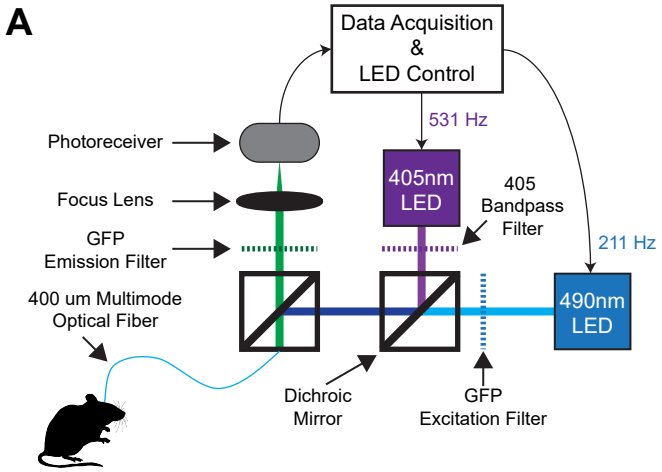

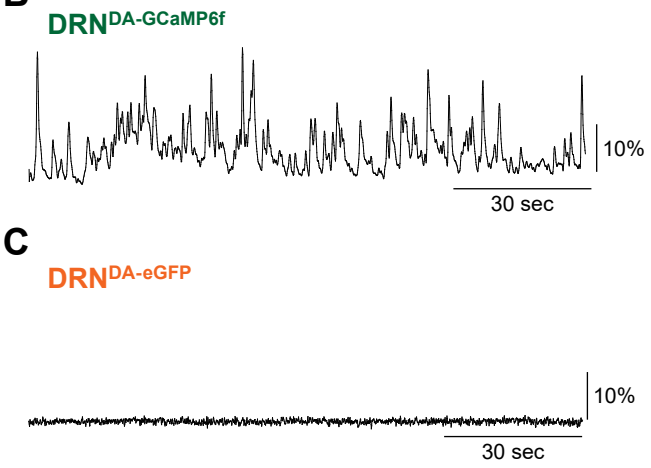

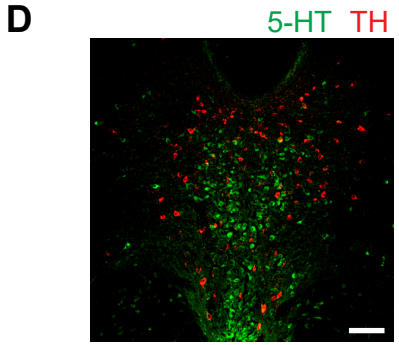

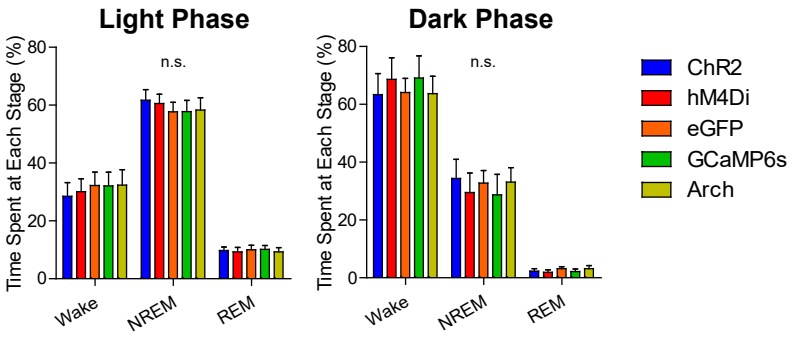

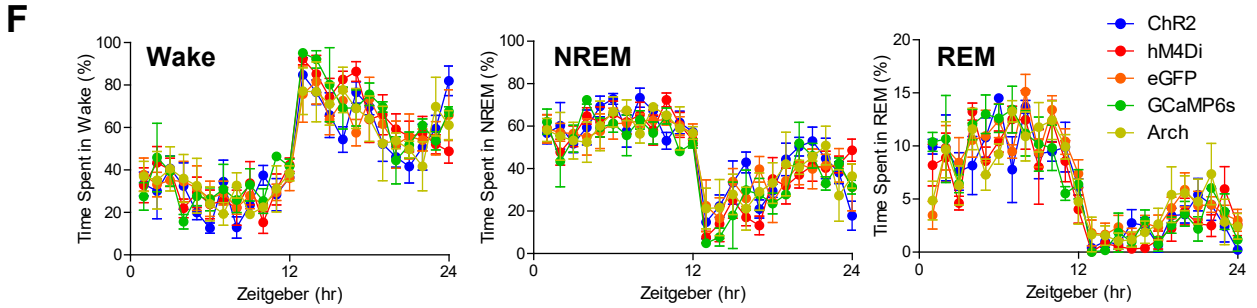

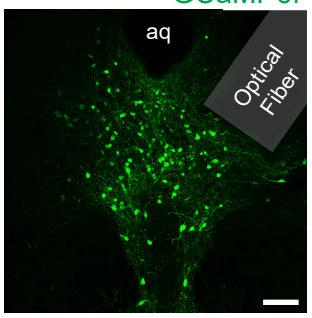

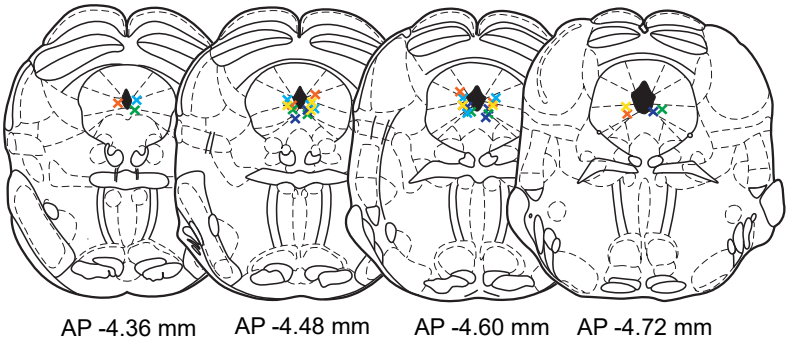

× DA-GCaMP6f × DA-GCaMP6s × DA-ChR2 × DA-eGFP × DA-eArch3.0

Figure S2

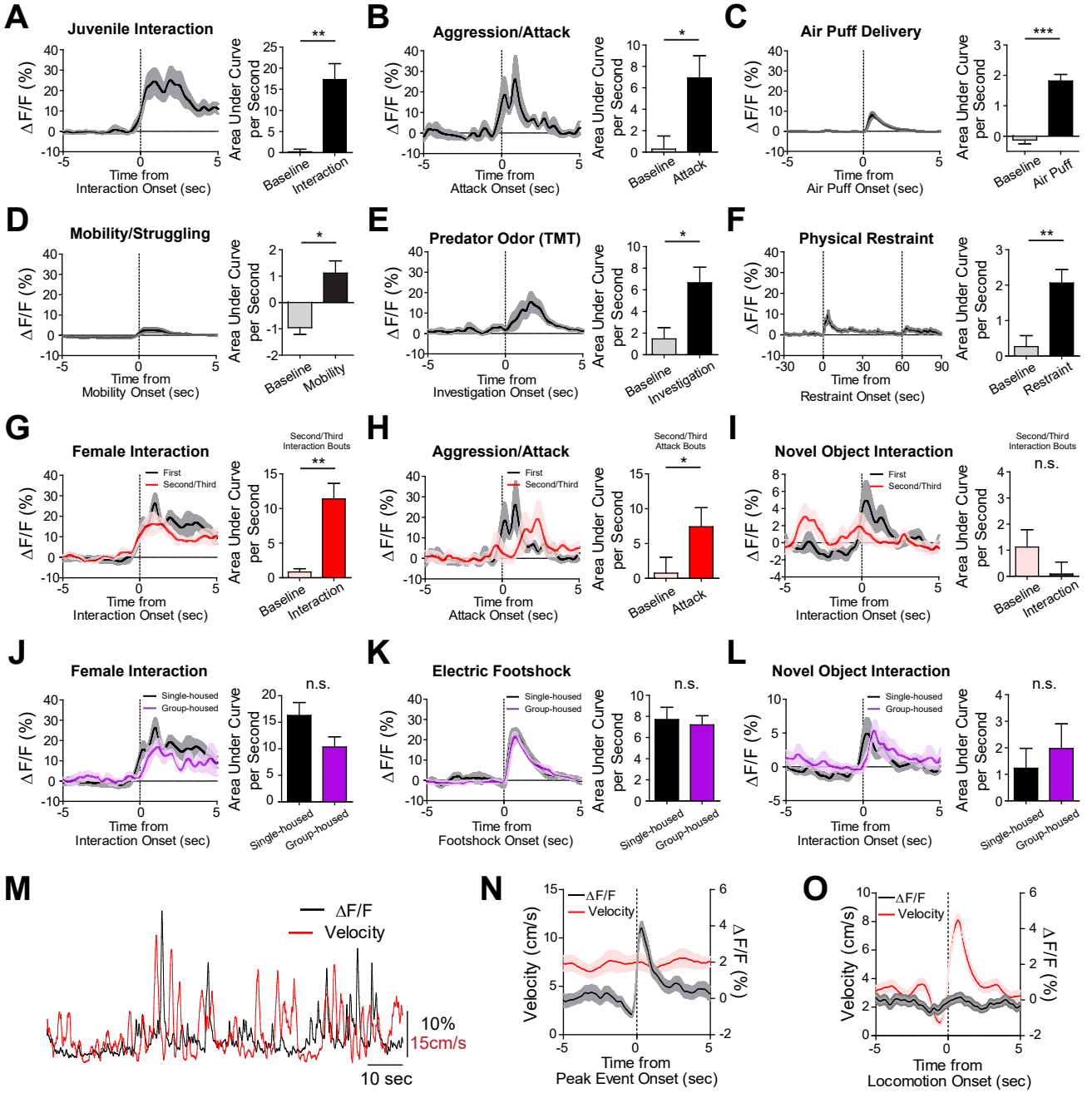
A
Juvenile Interaction
ΔF/F (%)
Time from Interaction Onset (sec)
Area Under Curve per Second
Baseline
Interaction
**
B
Aggression/Attack
Time from Attack Onset (sec)
Attack
*
C
Air Puff Delivery
Time from Air Puff Onset (sec)
Air Puff
***
D
Mobility/Struggling
Time from Mobility Onset (sec)
Mobility
E
Predator Odor (TMT)
Time from Investigation Onset (sec)
Investigation
F
Physical Restraint
Time from Restraint Onset (sec)
Restraint
**
G
Female Interaction
First
Second/Third
Second/Third Interaction Bouts
H
Aggression/Attack
Second/Third Attack Bouts
I
Novel Object Interaction
n.s.
J
Female Interaction
Single-housed
Group-housed
K
Electric Footshock
Time from Footshock Onset (sec)
L
Novel Object Interaction
M
ΔF/F
Velocity
10%
15cm/s
10 sec
N
Velocity (cm/s)
ΔF/F (%)
Time from Peak Event Onset (sec)
O
Time from Locomotion Onset (sec)

Figure S3

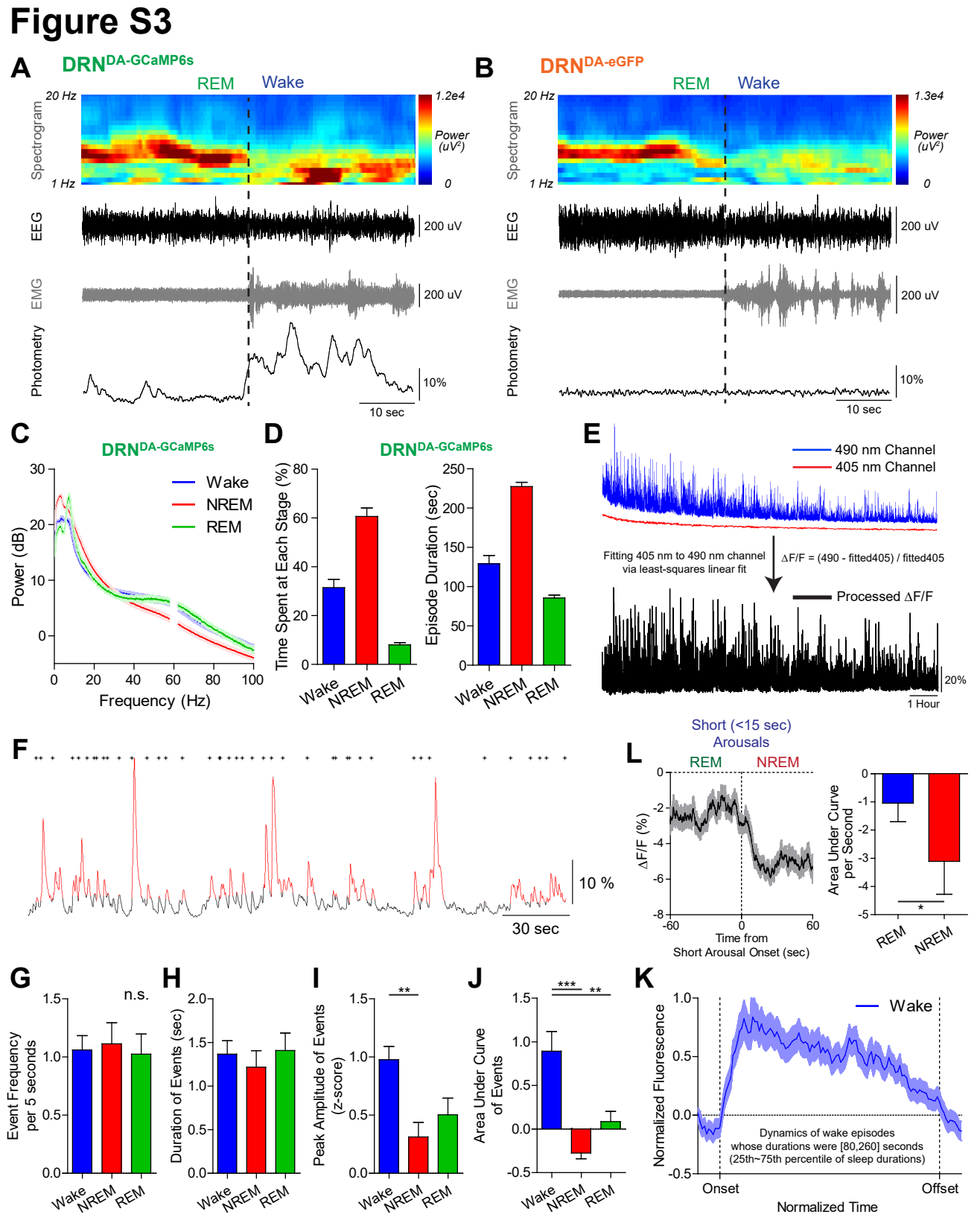
A
DRN DA-GCaMP6s
REM
Wake
Spectrogram
20 Hz
1 Hz
1.2e4
Power (uV²)
0
EEG
200 uV
EMG
200 uV
Photometry
10%
10 sec
B
DRN DA-eGFP
REM
Wake
Spectrogram
20 Hz
1 Hz
1.3e4
Power (uV²)
0
EEG
200 uV
EMG
200 uV
Photometry
10%
10 sec
C
DRN DA-GCaMP6s
Wake
NREM
REM
Power (dB)
Frequency (Hz)
D
DRN DA-GCaMP6s
Time Spent at Each Stage (%)
Episode Duration (sec)
Wake
NREM
REM
E
490 nm Channel
405 nm Channel
Fitting 405 nm to 490 nm channel via least-squares linear fit
ΔF/F = (490 - fitted405) / fitted405
Processed ΔF/F
20%
1 Hour
F
10 %
30 sec
L
Short (<15 sec) Arousals
REM
NREM
ΔF/F (%)
Time from Short Arousal Onset (sec)
Area Under Curve per Second
REM
NREM
*
G
n.s.
Event Frequency per 5 seconds
Wake
NREM
REM
H
Duration of Events (sec)
Wake
NREM
REM
I
**
Peak Amplitude of Events (z-score)
Wake
NREM
REM
J
***
**
Area Under Curve of Events
Wake
NREM
REM
K
Wake
Normalized Fluorescence
Dynamics of wake episodes whose durations were [80,260] seconds (25th~75th percentile of sleep durations)
Onset
Offset
Normalized Time

Figure S4

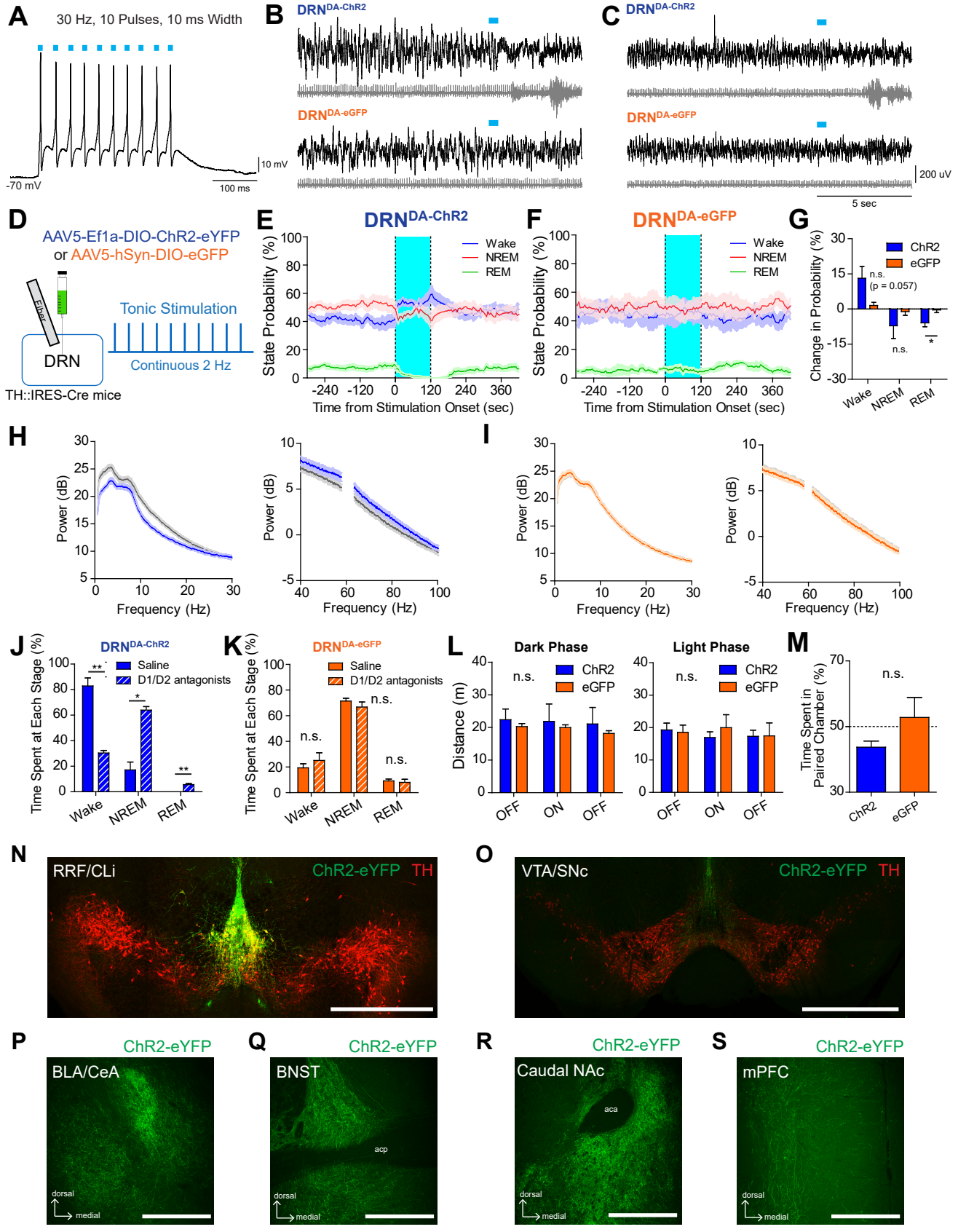
A
30 Hz, 10 Pulses, 10 ms Width
-70 mV
10 mV
100 ms
B
DRNDA-ChR2
DRNDA-eGFP
C
DRNDA-ChR2
DRNDA-eGFP
200 uV
5 sec
D
AAV5-Ef1a-DIO-ChR2-eYFP
or AAV5-hSyn-DIO-eGFP
Fiber
DRN
Tonic Stimulation
Continuous 2 Hz
TH::IRES-Cre mice
E
DRNDA-ChR2
State Probability (%)
Wake
NREM
REM
Time from Stimulation Onset (sec)
F
DRNDA-eGFP
State Probability (%)
Wake
NREM
REM
Time from Stimulation Onset (sec)
G
Change in Probability (%)
ChR2
eGFP
n.s.
(p = 0.057)
n.s.
*
Wake
NREM
REM
H
Power (dB)
Frequency (Hz)
Power (dB)
Frequency (Hz)
I
Power (dB)
Frequency (Hz)
Power (dB)
Frequency (Hz)
J
DRNDA-ChR2
Time Spent at Each Stage (%)
Saline
D1/D2 antagonists
**
*
**
Wake
NREM
REM
K
DRNDA-eGFP
Time Spent at Each Stage (%)
Saline
D1/D2 antagonists
n.s.
n.s.
n.s.
Wake
NREM
REM
L
Dark Phase
Light Phase
Distance (m)
n.s.
ChR2
eGFP
OFF
ON
OFF
M
Time Spent in Paired Chamber (%)
n.s.
ChR2
eGFP
N
RRF/CLi
ChR2-eYFP
TH
O
VTA/SNc
ChR2-eYFP
TH
P
ChR2-eYFP
BLA/CeA
dorsal
medial
Q
ChR2-eYFP
BNST
acp
dorsal
medial
R
ChR2-eYFP
Caudal NAc
aca
dorsal
medial
S
ChR2-eYFP
mPFC
dorsal
medial

Figure S5

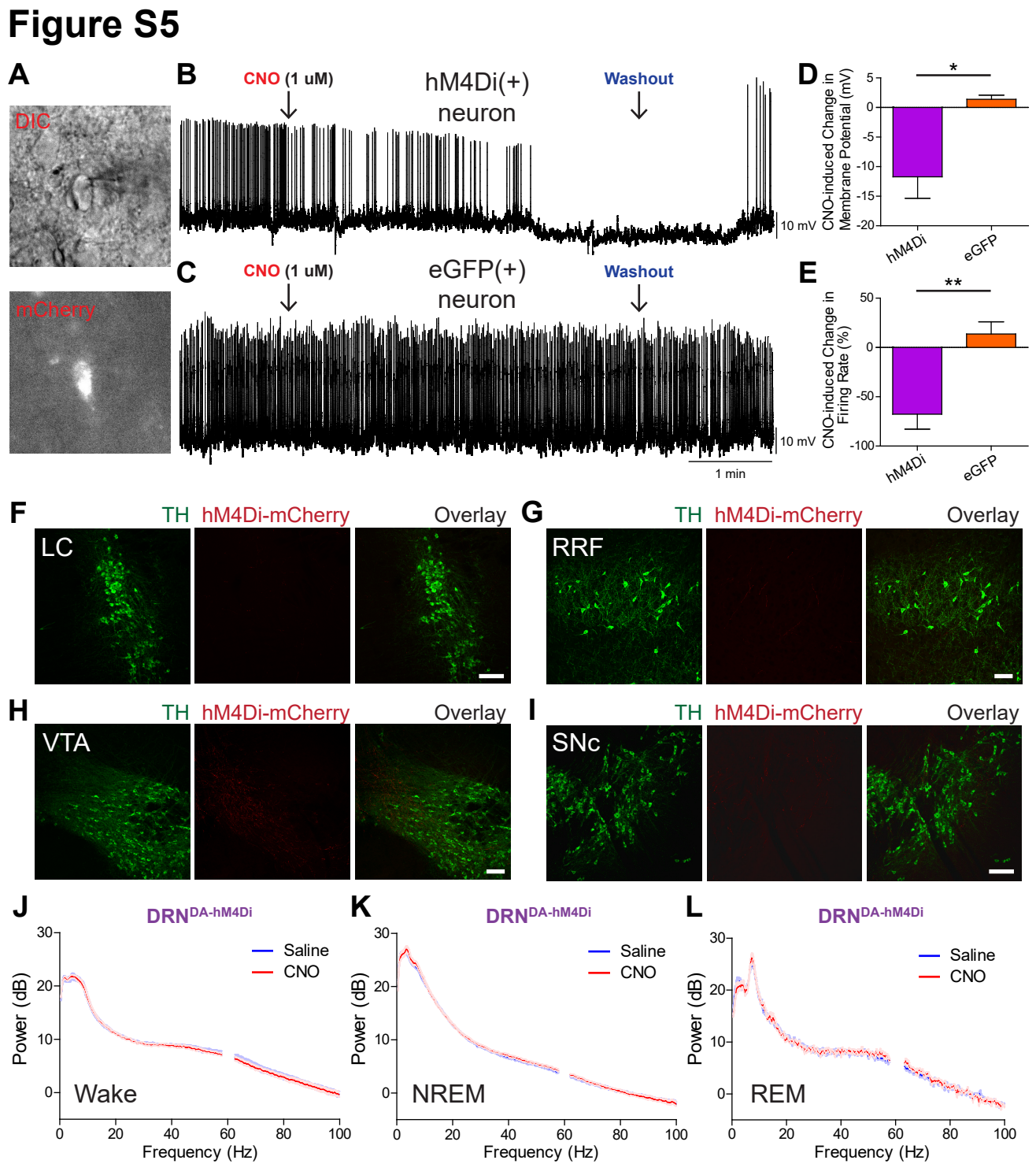
A
DIC
mCherry
B
CNO (1 uM)
hM4Di(+)
neuron
Washout
10 mV
C
CNO (1 uM)
eGFP(+)
neuron
Washout
10 mV
1 min
D
CNO-induced Change in Membrane Potential (mV)
5
0
-5
-10
-15
-20
*
hM4Di
eGFP
E
CNO-induced Change in Firing Rate (%)
50
0
-50
-100
**
hM4Di
eGFP
F
TH
hM4Di-mCherry
Overlay
LC
G
TH
hM4Di-mCherry
Overlay
RRF
H
TH
hM4Di-mCherry
Overlay
VTA
I
TH
hM4Di-mCherry
Overlay
SNc
J
DRNDA-hM4Di
Saline
CNO
Power (dB)
30
20
10
0
Wake
0
20
40
60
80
100
Frequency (Hz)
K
DRNDA-hM4Di
Saline
CNO
Power (dB)
30
20
10
0
NREM
0
20
40
60
80
100
Frequency (Hz)
L
DRNDA-hM4Di
Saline
CNO
Power (dB)
30
20
10
0
REM
0
20
40
60
80
100
Frequency (Hz)

Figure S6

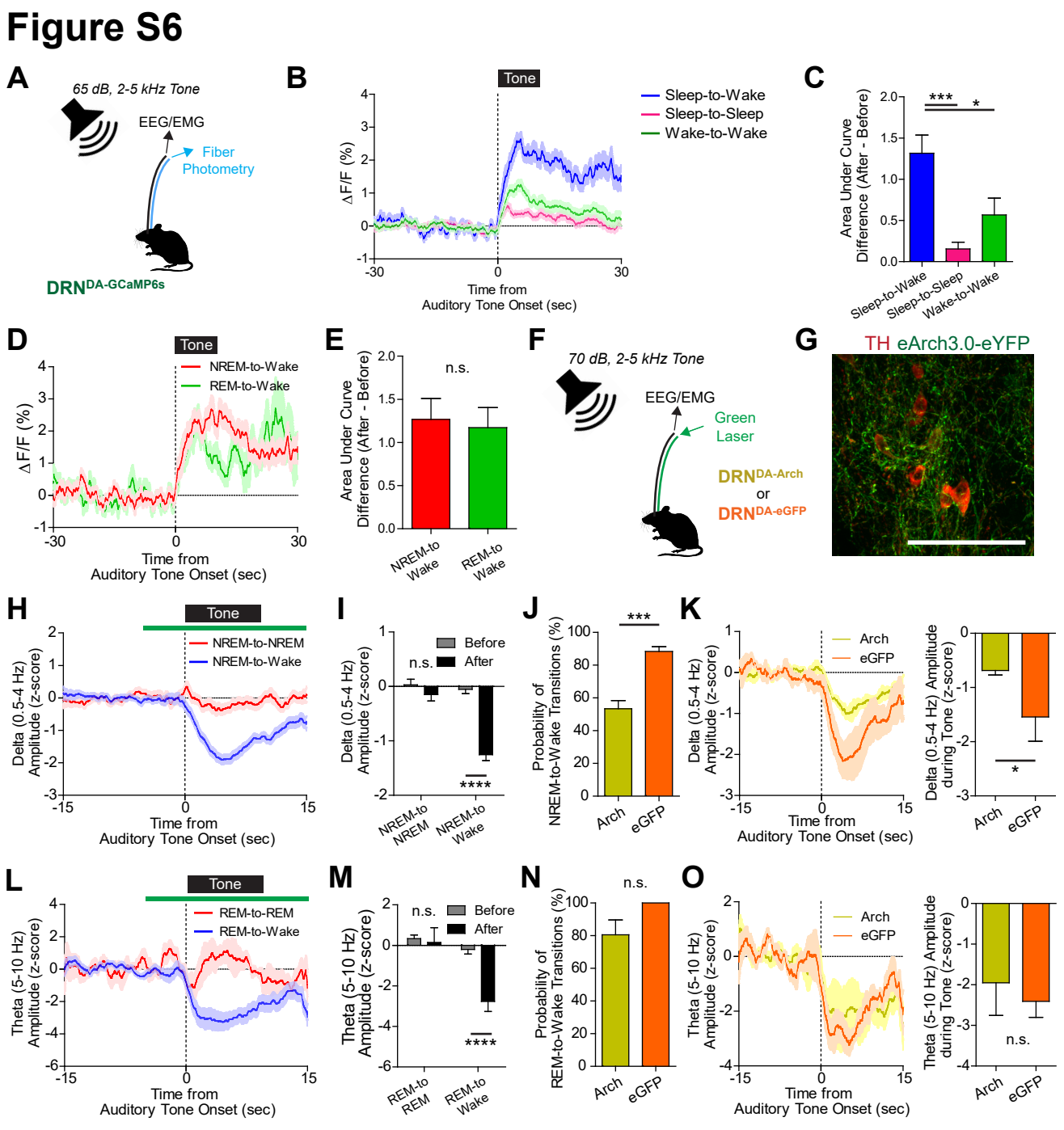
A
65 dB, 2-5 kHz Tone
EEG/EMG
Fiber Photometry
DRNDA-GCaMP6s
B
Tone
ΔF/F (%)
Time from Auditory Tone Onset (sec)
Sleep-to-Wake
Sleep-to-Sleep
Wake-to-Wake
C
Area Under Curve Difference (After - Before)
***
*
Sleep-to-Wake
Sleep-to-Sleep
Wake-to-Wake
D
Tone
NREM-to-Wake
REM-to-Wake
ΔF/F (%)
Time from Auditory Tone Onset (sec)
E
Area Under Curve Difference (After - Before)
n.s.
NREM-to Wake
REM-to Wake
F
70 dB, 2-5 kHz Tone
EEG/EMG
Green Laser
DRNDA-Arch
or
DRNDA-eGFP
G
TH eArch3.0-eYFP
H
Tone
NREM-to-NREM
NREM-to-Wake
Delta (0.5-4 Hz) Amplitude (z-score)
Time from Auditory Tone Onset (sec)
I
Before
After
n.s.
****
Delta (0.5-4 Hz) Amplitude (z-score)
NREM-to NREM
NREM-to Wake
J
***
Probability of NREM-to-Wake Transitions (%)
Arch
eGFP
K
Arch
eGFP
Delta (0.5-4 Hz) Amplitude (z-score)
Time from Auditory Tone Onset (sec)
Delta (0.5-4 Hz) Amplitude during Tone (z-score)
*
Arch
eGFP
L
Tone
REM-to-REM
REM-to-Wake
Theta (5-10 Hz) Amplitude (z-score)
Time from Auditory Tone Onset (sec)
M
Before
After
n.s.
****
Theta (5-10 Hz) Amplitude (z-score)
REM-to REM
REM-to Wake
N
n.s.
Probability of REM-to-Wake Transitions (%)
Arch
eGFP
O
Arch
eGFP
Theta (5-10 Hz) Amplitude (z-score)
Time from Auditory Tone Onset (sec)
Theta (5-10 Hz) Amplitude during Tone (z-score)
n.s.
Arch
eGFP